

Neuronal-like Irregular Spiking Dynamics in Highly Volatile Memristive Intermediate-scale AgPt-Nanoparticle Assemblies

Niko Carstens, Thomas Strunskus, Franz Faupel, Abdou Hassanien,* and Alexander Vahl*

Neuromorphic computing seeks functional materials capable of emulating brain-like dynamics to solve computational problems with time and energy efficiency, outclassing current transistor-based hardware architectures. Major efforts are focused on integrating memristive devices into highly regular circuits (i.e., crossbar arrays), where the information representation in individual memristive devices is closely oriented toward the behavior of artificial neurons. However, artificial neurons are rather rigid mathematical concepts than realistic projections of complex neuronal dynamics. Neuroscience suggests that highly efficient information representation on the level of individual neurons relies on dynamical features such as excitatory and inhibitory contributions, irregularity of firing patterns, and temporal correlations. Here, a conductive atomic force microscopy approach is applied to probe the memristive dynamics of nanoscale assemblies of AgPt-nanoparticles at the stability border of the conducting state, where physical forces causing the formation and decay of filamentary structures appear to be balanced. This unveils a dynamic regime, where the memristive response is governed by irregular firing patterns. The significance of such a dynamical regime is motivated by close similarities to excitation and inhibition-governed behavior in biological neuronal systems, which is crucial to tune biological neuronal systems into a state most suitable for information representation and computation.


1. Introduction

Technical implementation of computational principles from complex neuronal assemblies such as mammalian brains is currently the focus of the search for unconventional hardware approaches, which aims to overcome fundamental limitations set by modern transistor-based hardware technology, such as limited miniaturization capabilities or the von-Neumann bottleneck.^[1] Closely connected to this is the development of memristive devices, which embody two-terminal resistive switching elements with non-linear dynamical behavior.^[2] The major significance of memristive devices is their ability to implement synaptic-like functionalities in technical circuits through their reconfigurable conductance.^[3–6] Current approaches for the implementation of brain-inspired computation paradigms are mostly focused on highly regular crossbar arrays of memristive devices, e.g., with the intent of applications for in-memory computing, for vector-matrix multiplication in mixed-precision hardware imple-

mentations and many more.^[7,8] Despite substantial advances in this technology, which was mainly driven by opportunities to perform artificial neural network algorithms directly from the underlying physics of memristor crossbar arrays,^[9–11] it is still away from reaching a level of brain-like complexity with emergent dynamical features as found in biological neuronal systems.^[12] One reason for this is that design principles for memristive devices are commonly oriented toward rather rigid mathematical constructs, effectively modeling isolated aspects of synaptic or neuronal behavior omitting the full complexity of a realistic biological neuron. In contrast to that, the computational capabilities of biological neuronal systems trace back to their reconfigurable connectivity, dynamical synaptic features, and spatio-temporal plasticity, with all of these aspects being inseparably interwoven. These complex networks incorporate rich adaptability mechanisms on the local level (i.e., on the level of individual synapses and neurons), which allows the whole network to self-organize into a regime that is functional for information representation and processing.^[13] Some functional principles found on the local level of biological neuronal

N. Carstens, T. Strunskus, F. Faupel, A. Vahl
Institute for Materials Science
Chair for Multicomponent Materials
Faculty of Engineering
Christian-Albrechts-University of Kiel
Kaiserstraße 2, D-24143 Kiel, Germany
E-mail: alva@tf.uni-kiel.de

A. Hassanien
Department of Condensed Matter Physics
J. Stefan Institute
Jamova 39, Ljubljana 1000, Slovenia
E-mail: abdou.hassanien@ijs.si

 The ORCID identification number(s) for the author(s) of this article can be found under <https://doi.org/10.1002/ppsc.202200131>.

© 2023 The Authors. Particle & Particle Systems Characterization published by Wiley-VCH GmbH. This is an open access article under the terms of the Creative Commons Attribution-NonCommercial License, which permits use, distribution and reproduction in any medium, provided the original work is properly cited and is not used for commercial purposes.

DOI: 10.1002/ppsc.202200131

systems are, among others, balancing excitatory and inhibitory synaptic contributions to signal processing^[14–16] or modulation of synaptic signal transmission efficiency^[17] on short- and long-term scales. In particular, for an efficient representation of information, which is present in biological systems in the form of irregular spike trains, the interplay between excitatory and inhibitory contributions has major importance.^[18,19] The combination of local neuronal and synaptic behavior along with the complex network connectivity are leading to emergent dynamics, which are considered as crucial for the computational capabilities of the brain.^[12,13] Taking these aspects as an inspiration, there are recent approaches to build neuromorphic systems which focus more on experimental findings from neuroscience and less on artificial neural network algorithms. For example, long-range temporal correlations and scale-free avalanches (both are well-described dynamics governing the spontaneous activity of biological neuronal systems^[12,20,21]) were implemented in randomly assembled networks of metallic nanowires^[22] or nanoparticles.^[23–25] This allows for the creation of neuromorphic systems approaching brain-like complexity in the dynamics, which are beneficial for the mapping of spatio-temporal information and therefore believed to be suitable for computational schemes like reservoir computing.^[26,27] Furthermore, diffusive memristive switching attracted interest for the implementation of enhanced synaptic functionalities in neuromorphic systems.^[28–30] The characteristic feature of a diffusive memristor is the volatility of the conducting state, which originates from permanently acting relaxation forces driven by interfacial energy minimization, causing spontaneous decay of conductive filaments.^[31] Diffusive memristors in a conventional sense implement a highly non-linear threshold behavior, characterized by a certain threshold voltage V_T . When a voltage $V > V_T$ is applied, a diffusive memristor occupies its conducting state, otherwise it relaxes back to its insulating state.^[32] Based on the inherent volatility, functionalities like short-term plasticity^[30] and regular spike-pattern generators^[33] can be deduced, which are both important contributions to creating neuromorphic systems inspired by the real behavior of biological neuronal systems.

Pathways for the imitation of the realistic complex behavior of individual biological neurons toward emulation of excitatory and inhibitory contributions were not pursued so far. However, this would open up new approaches for the design of neuromorphic systems with a close orientation toward biological neuronal systems. One major reason why biological neuronal systems adapt excitatory and inhibitory contributions is to maximize the dynamical range,^[18,34,35] a parameter that is crucial for computational capabilities.^[13,36] To explore pathways, that allow emulating principles of biological excitatory and inhibitory contributions, we investigated the dynamics of a memristive system built by an intermediate-scale AgPt nanoparticle (NP) assembly. Here, the term “intermediate-scale” is used in order to discriminate the AgPt NP arrangement on the one hand against “large-scale”, interconnected NP networks at the percolation threshold, which exhibit collective switching properties such as avalanche dynamics, and on the other hand against “low-scale” nanocomposites with sparse distribution of nanoparticles inside a dielectric matrix, which typically exhibit conventional diffusive memristive switching. To study the memristive switching dynamics

in intermediate-scale AgPt NP assemblies, in this work the full memristive stack was integrated directly into the apex region of a conductive cantilever. This functionalized cantilever was used to probe the current response upon application of a voltage stimulus over prolonged times via a common conductive atomic force microscopy (cAFM) setup. The main advantage of using this unconventional cAFM approach is an efficient localization of the memristive action of the intermediate-scale AgPtNP assembly to the cantilever apex, which enables long-term measurements on memristive switching phenomena, their dynamics, and their temporal correlations. This approach already proved well for probing the dynamics on longer time scales of an individual Ag-filament evolved from a thin film electrode (full details of this previous study can be found elsewhere^[37]). While the abovementioned cAFM-related approach targets fundamental studies on long-term, highly localized, filamentary switching, there are also approaches that intend to bring cone-like to tip-like structures to the fabrication of memristive devices on chip and wafer levels.^[38–40]

With an intermediate-scale AgPt NP assembly at the apex of a cAFM cantilever, in this study it was possible to constrain the memristive system to a highly volatile switching regime (in the nA range) which is strongly governed by repeated decays of the conducting state, leading to the emergence of irregular spiking patterns, resembling the firing activity of neurons in biological systems. With these fundamental investigations of highly volatile resistance states and the dynamical transitions therein, this study provides first indications that link the balance of physical forces causing the formation and spontaneous decay of filamentary structures to excitatory or inhibitory-like contributions and as such unveils novel perspectives for the design of future neuromorphic systems.

2. Design of Memristive Test System and Operation Conditions

AgPt NPs were chosen in this work for the formation of the memristive system. Such bimetallic NPs were already reported to be feasible for the stable implementation of diffusive memristive switching on the nanoscale.^[32] For the studies in this work, we made use of an unconventional cAFM approach, which already proved beneficial for the investigation of diffusive memristive dynamics of nanoscale Ag-filaments.^[37] This approach implies a persistent integration of the memristive system directly at the cantilever apex, instead of conventional cAFM probing. Following this approach, the test system for this work is a cantilever functionalized with a memristive system of AgPt NPs encapsulated in an insulating matrix consisting of SiO_xN_y . This test system was fabricated by taking a commercially available Pt-covered cantilever (Bruker CONTV-PT) and successive coating starting with 5 nm SiO_xN_y , followed by AgPt-NPs and finally a 5 nm SiO_xN_y covering. A schematic depiction of the memristive stack on the memtip cantilever as well as the test system is given in **Figure 1a,b**, respectively. An scanning electron microscopy (SEM) micrograph depicting the apex region of the memtip cantilever is shown in **Figure 1c**. Additional SEM images of the functionalized cantilever can be found in Supporting Information S1.

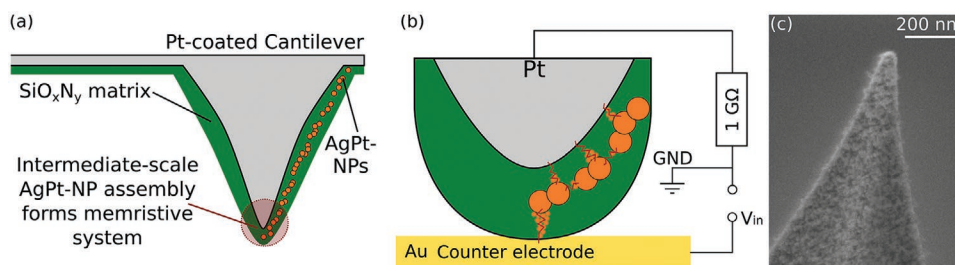


Figure 1. Illustration of the memtip cantilever layout and test system. a) The memristive dynamics of a nanoscale assembly of AgPt-NPs are probed via an unconventional cAFM approach, where the memristive system consisting of AgPt-NPs encapsulated in an insulating SiO_xN_y matrix is persistently integrated at the cantilever tip. By this, the memristive action of AgPt NPs is efficiently constrained to the electrical field-enhanced apex area with the intention to avoid experimental uncertainties induced by thermal drift and lacking localizability of memristive action. b) The cantilever with an integrated memristive system is brought into contact to an Au counter electrode and probed via voltage ramps. Memristive action is triggered in the apex area causing field-induced rearrangements of Ag atoms within the SiO_xN_y matrix and measured conductance depends on the configuration of potential switching gaps. Potential filamentary-type switching gaps are indicated by red zigzag lines. c) A SEM micrograph of the cantilever decorated with AgPt NPs, recorded at the apex of the memtip cantilever.

Resulting from the cantilever functionalization, the studied memristive system can be understood as an intermediate-scale assembly of AgPt NPs. Reservoirs of mobile species from which filamentary structures are formed (i.e., Ag) are distributed over the location of NPs. Furthermore, each gap between adjacent NPs could contribute to the memristive response of the system. The according scale of the memristive system is defined by the geometry of the apex region, i.e., it is determined by the active area during cAFM measurements. The scale of the memristive system can be estimated from the order of the apex curvature radius, that is 25 nm according to the specifications of the used cantilever model. From this, it can be expected that the memristive systems extend over multiple AgPt NPs and that the response of the system includes the memristive activity of several nanogaps across the system. Characterizations were done by establishing a contact between the cantilever with an integrated memristive system and an Au surface (as a typical representative for an inert counter electrode) and conduction of voltage sweep experiments. Taking Au as a back electrode, we expect ohmic contacts between the evolving filaments and back electrode material.^[37] Figure 1b illustrates the experimental scenario designed in this work. The advantage of using a functionalized cantilever as a memristive test system is, that it creates stable conditions regarding the nanoscale positioning of probe and sample. Therefore, any stochastic drift (e.g., induced by thermal motion) between cantilever and memristive system consisting of AgPt-NPs, which would impose considerable experimental uncertainties during longer measurements,^[41,42] are mitigated. Due to the inherent electrical field enhancement, the memristive action is efficiently constrained to the cantilever apex, which reduces uncertainties with respect to spatial localization of memristive action. Consequently, this ensures that the observed memristive action originates consistently from the same intermediate-scale AgPt NP assembly. We took three different measures to establish operation conditions, which drive the AgPt NP system into a highly volatile switching regime. Firstly, AgPt alloy NPs were deliberately chosen to achieve a strict limitation of active species. Pt as a noble metal remains electrochemically inert and resides as immobile anchor points in the system, whereas only the Ag-fraction contributes to the formation of filamentary structures. Second, a serial 1 GΩ

resistor was integrated into the measurement circuit. This strongly restricts the (Ag^+ -ion based) material transport and avoids the formation of persistent conducting paths, which arise when the diameter of filamentary structures approaches the regime of long-term stable filaments.^[31] Lastly, we stimulated the system with a regular triangular voltage signal with amplitudes of 1 V and -2.5 V to include lower-bias periods, allowing the system to relax repeatedly, which turned out to be non-destructive for longer measurements.

3. Results

The utilization of a cantilever with an integrated memristive system consisting of AgPt NPs encapsulated in SiO_xN_y , together with the operation conditions as described above, proved to be suitable to investigate the dynamics in a highly volatile regime. We operated the intermediate-scale AgPt-NP assembly over 8000 repeating voltage cycles, where a considerable fraction of cycles exhibited switching patterns, as represented in **Figure 2a**. Regarding the positive polarity, throughout the measurement series, we restricted the applied bias to be below the threshold of memristive switching (the 1 V amplitude at positive polarity does not induce sufficient driving force to overcome the activation barriers in the underlying memristive switching kinetics^[43,44]). Such a threshold behavior is commonly observed in diffusive switching devices, hence, periods with positive polarity had a sub-threshold character, where forces leading to decay of conducting states are prominently acting on the AgPt NP system. At periods with negative polarity, sufficient driving forces exist to form filamentary structures and to trigger transitions into conducting states. It can be seen, that the AgPt NP system responded via complex switching patterns, governed by several switching events accompanied by repetitive decay of conducting states. This is indicative of the high volatility of the conducting states established by this operation regime. Details on the physical mechanisms which are manipulating the states of the AgPt NP system and its conductivity are treated in the discussion part. We note, that not the entire amount of measured cycles exhibited such a complex switching pattern. Among the entire measurement, there are also many cycles

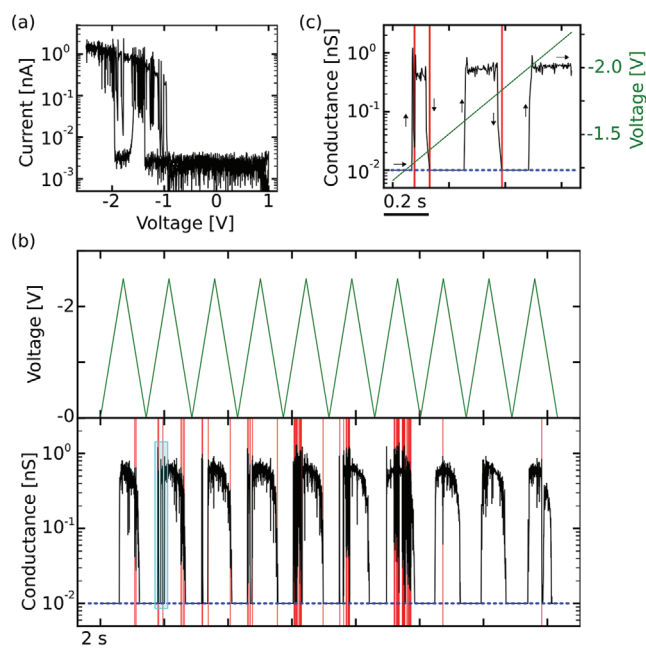


Figure 2. Representation of highly volatile memristive switching dynamics of the intermediate-scale AgPt NP assembly. a) A representative IV-diagram showing the current response upon triangular voltage stimulation. At negative polarity, the threshold region for transitions into conducting states is reached, where the memristive dynamics are governed by irregular fluctuations between insulating and conducting states. A more detailed illustration of the switching events in this cycle is shown in Supporting Information S4. The observed repeating decays of the conducting state are denoted in the frame of this work as “inhibitory-like” spiking events (ISEs). b) Alternative illustration of ISEs via plotting conductance versus time for ten consecutive cycles. For better readability, all data points belonging to positive polarity are omitted and each conductance value lower than 0.01 nS is cropped to the level of 0.01 nS (blue dotted line, limited by the measurement resolution and representing the insulating state of the memtip). Detected (see Experimental Section) ISEs are indicated by red vertical lines. c) shows a sequence of ISEs within a single measurement cycle, corresponding to a magnified view of the cyan box in (b).

included that show the dynamics of a conventional diffusive memristor, as shown in Supporting Information S2. Additionally, many measurement cycles suggest, that the intermediate-scale AgPt NP assembly can occupy multiple conductive states. A typical example of this is shown in Supporting Information S3. An alternative illustration of the highly volatile memristive dynamics is given in Figure 2b, showing the memristive response from sequential cycles in terms of conductance of the AgPt-NP system in series with the 1G Ω resistor versus time. From this, it can be seen that the memristive response partially resembles that of a diffusive memristor, i.e., there are clear threshold switching events between the insulating and conducting states and at zero-bias conditions, there is only an insulating state present. However, the complexity of memristive dynamics described here goes beyond to that of a conventional diffusive memristor. That is, because, at voltages that are higher than the threshold for the transition into conducting states, there is a certain probability for a spontaneous decay of the conducting state, whereas for a conventional diffusive memristor a permanent occupation of the conducting state is assumed.

A magnified view in Figure 2c shows a more clear illustration. Despite increasing voltage stimulation, switching into the conducting state is not permanent above the threshold voltage, but superimposed by repetitive spontaneous decays, as indicated by the vertical red lines in the figure. The vast majority of these repetitive decays appeared to be threshold-like, i.e., the transitions between insulating and conducting states (and also vice versa) occurred within time scales in the order of the temporal resolution during the measurement (1.2 milliseconds) or below. These dynamical features, evoked by highly volatile operation conditions, goes beyond the dynamics of conventional diffusive memristors.^[30,32]

Overall, the dynamics exhibited by the AgPt NP system are expressed by irregular fluctuations between insulating and conducting states. In this regard, there is a close resemblance to neuronal spiking patterns in biological systems.^[45–47] We note, that our system is not equivalent to spike pattern generation via a relaxation oscillator circuit realized with a diffusive memristor, like in.^[33] Relaxation oscillator circuits implement regular spiking patterns with the aid of an external capacitance (which allows to regulate spiking frequencies), whereas the spiking in the memtip system has a more probabilistic nature. In biological neuronal systems, information is encoded on the level of individual neurons by irregular trains of voltage spikes, emerging from excitatory and inhibitory signal inputs coming from adjacent neurons.^[46] For biological neuronal systems, it is important to maintain balanced contributions of excitatory and inhibitory inputs, to achieve optimum capabilities to represent and process information.^[13] We propose that the highly volatile switching regime of the intermediate-scale AgPt NP assembly is able to emulate the balanced state of excitatory and inhibitory contributions known from individual neurons and therefore offers similarities to the information encoding scheme as known from biological neuronal systems. This will be argued more deeply in the discussion part. In order to characterize the irregular conductance fluctuations in the highly volatile operation regime more deeply, we introduce the term “inhibitory-like” spiking event (ISE) as an edge, where a conducting state of the AgPt NP system spontaneously decays (see red vertical lines in Figure 2b,c). A function in Python was written to detect ISEs in the whole measurement, where an ISE was detected as a monotonic decrease of conductivity by at least one order of magnitude. Following this definition, $\approx 20.5\%$ of all measurement cycles had at least 2 detected ISEs, i.e., they had an increased dynamical complexity compared to conventional diffusive switching. The count statistics of ISEs for the whole measurement over 8000 cycles can be found in greater detail in the histogram in Figure 3a. Here, the distribution of cycles with different numbers of detected ISEs is shown. The distribution indicates that there is a higher abundance in cycles with a few ISEs and with increasing number of ISEs the distribution falls off until it drops $\approx 10^2$ ISEs per cycle. The temporal sequence of number of ISEs in an individual measurement cycle is shown as a plot against cycle number in Figure 3b. Here, it is observed that the number of ISEs per cycle varies between cycles with only one ISE and cycles with up to 104 ISEs. The distribution of the variation in the ISE occurrence implies that the degree of activity (in terms of number of ISEs) has a temporally correlated nature. This follows from the observation, that cycles

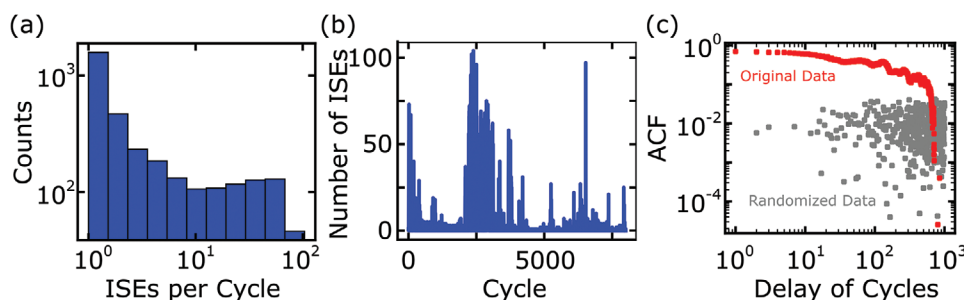


Figure 3. Count statistics of ISEs detected in individual measurement cycles and autocorrelation behavior. a) histogram plot (logarithmic bin widths) exhibiting the count of measurement cycles in dependence on the number of ISEs detected within an individual cycle. b) temporal evolution of ISE activity as a bar plot of number of ISEs detected in an individual cycle versus cycle number. c) autocorrelation function (ACF) calculated for the sequence of spike counts in (b), shown in red, indicates temporal correlations, meaning that cycles with a high/low number of ISEs are followed by cycles with again high/low number of ISEs. The grey data points plot the ACF when the sequence of spike counts is shuffled, indicating the destruction of temporal correlations.

with a high number of ISEs appear to occur accumulated and not evenly distributed over the whole sequence of measurements. The autocorrelation function (ACF)^[48] calculated from the sequence of ISEs per cycle reveals the presence of temporal correlations, as shown in Figure 3c. In Figure 3c, the correlation of the number of ISEs of one measurement cycle with respect to the previous cycles (delay) is depicted. The correlation is high for low delays, i.e., for neighboring measurement cycles, which indicates, that cycles with a high/low number ISEs are likely to be followed by cycles with again a high/low number of ISEs. The autocorrelation breaks down in case the original data are shuffled (randomized data in Figure 3c). The fact that dynamical features of the volatile switching regime show autocorrelation behavior fit with earlier studies on Ag-based memristive nanostructures.^[37] Under the assumption, that the spike count within a cycle is substantially determined by the momentary morphology of the intermediate-scale AgPt NP assembly (i.e., momentary Ag-mass distribution in the system), the occurrence of autocorrelation behavior can be explained from timescales that govern significant morphological changes. Autocorrelations in the switching dynamics occur when the timescales for significant morphological changes (which have a major influence on the ISE count) are larger than the time for one measurement cycle. Based on this, the dynamics of consecutive cycles are similar, and considerably different spike counts mainly arise when the measurement has proceeded over a larger amount of cycles.

Furthermore, we characterized the temporal structure of ISEs within individual cycles by means of the probability distribution of inter-event intervals (IEIs). One IEI was defined as time between subsequent ISEs occurring within one measurement cycle. Therefore, only measurement cycles showing at least 2 ISEs contributed to the IEI evaluation. The probability density function (PDF) represented on a log-log scale of all detected IEIs is shown in Figure 4. It can be seen that the PDF has a skewed shape. Skewed shapes commonly originate from underlying lognormal statistics, which generally arise when the random variable (IEI in this case) is a consequence from multiplication of a multitude of other independent random variables.^[49] The occurrence of a skewed IEI distribution additionally supports dynamical similarities between spiking of biological neurons and the memristive AgPt NP system, because

neuronal firing rates result from various interacting processes and therefore frequently follow skewed distributions.^[49] For similar reasons, skewed distributions can be found in the dynamical features of filamentary switching systems.^[50,51] Here, we speculate that the skewed distribution of IEIs is a reflection of the multiple gap character on the intermediate-scale AgPt NP assembly, meaning that transitions between insulating and conducting state (and connected to this the detection of ISEs) require a multiplicative interplay^[49] of multiple gaps in the system.

4. Discussion

In the following discussion, we argue that the physical forces, which are acting on the intermediate-scale AgPt NP assembly and driving the highly volatile operation regime, can be categorized into excitatory-like and inhibitory-like contributions for meaningful reasons. Excitatory-like contributions include all physical forces that promote the formation of filamentary structures within the memristive system, whereas inhibitory-like contributions include all physical forces that cause the decay of filaments. We further argue that this closely resembles the interplay of excitatory and inhibitory synaptic inputs, which determines the dynamics on a local level in biological neuronal systems.^[14–16,35]

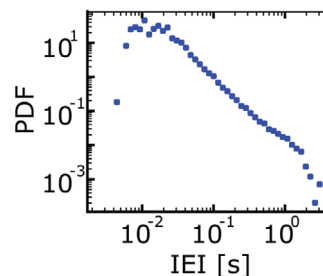


Figure 4. Temporal structure of ISEs within individual measurement cycles. Shown in the probability density function (PDF) of all time intervals between sequential ISEs (inter-event interval IEI) extracted from individual cycles. The PDF suggests a skewed shape.

4.1. Origin of Highly Volatile Switching Regime

Firstly, physical mechanisms that govern the observed irregular spiking behavior are discussed. Most fundamentally, the measured conductance reflects the internal distribution of Ag within the system.^[52] If there is a continuous metallic filament from cantilever apex to the Au counter electrode a conducting state is measured and, vice versa, the sample is in an insulating state when a continuous filament is missing. In analogy to the behavior of biological synapses,^[5,30] a conducting state of the memristive system corresponds to high information transmission, whereas there is no information transmission in an insulating state. For Ag-based memristive systems, electrochemical metallization is the dominating mechanism leading to the formation of filamentary structures.^[43,53] Triggered by the external electrical field across the memristive system, electrochemical oxidation of Ag occurs at anodic sites in the system, and Ag⁺-ions are released into the matrix. The Ag⁺-ions are able to migrate in the dielectric matrix (which is partially directed due to the external field) until they become reduced at cathodic sites in the system. Following these processes, a continuous metallic filament may be formed, causing a transition into a conducting state. Hence, the local electrical field, which relates to the external electrical potential constitutes a force driving the system into a conducting state, and therefore it can be seen to act excitatory-like on the memristive system. Filamentary structures in the memristive systems are destabilized by an increased amount of interfacial energy, causing spontaneous decay of filamentary structures.^[30,31] This is because filamentary structures possess a larger surface-to-volume ratio with high interfacial energy and the overall energy of the system can be minimized through decay of filaments into spherical clusters. In particular, according to this mechanism the volatile dynamics of a diffusive memristor, i.e., the presence of an insulating state at low bias conditions, can be explained by shorter retention times of thinner filaments. Generally, this driving force persistently acts against the formation of filamentary structures and limits their lifetime. Therefore, it can be considered to give inhibitory-like contributions to the AgPt NP system, i.e., it drives the system toward the insulating state. In the balance between the two abovementioned processes, the serial resistor plays an important role. The incorporation of the 1 GΩ serial resistor to the circuit limits the memtip's capability of retaining a stable filament and evokes additional filament instabilities, due to a voltage divider arrangement. After switching into a conducting state, the electrical field across the memristive system becomes strongly reduced (nearly the entire voltage now drops across the 1 GΩ resistor), meaning that the excitatory-like driving force (i.e., the electrical field across the memristive system) is inherently diminished, as soon as the memristive system reaches a conducting state. With this shift in the balance between the filament formation processes (excitatory contribution) and the filament dissolution processes (inhibitory contribution), the main difference to conventional metal cation-based filamentary memristors has to be pointed out: While the fundamental mechanisms of filament formation and disintegration are valid throughout different device classes, the balance between excitatory and inhibitory forces changes from stable bipolar devices over conventional diffusive devices

toward the highly volatile switching, which is described in this work. Depending on this balance, the filament lifetimes (i.e., retention time of conducting state) is consequently either much larger than the IV loop recording time (for bipolar memristive switching), similar (for conventional diffusive switching), or lower (for highly volatile switching), respectively. Similar to the memristive system in this work, Ag-based nanostructures have been previously reported in the context of diffusive memristive devices.^[28,30,32] In such conventional diffusive memristors, the operational regime has characteristic threshold voltages V_{SET} and V_{RESET} . These threshold voltages define a stable conducting regime (when voltages $V > V_{\text{SET}}$ are applied) and insulating regime (at voltages $V < V_{\text{RESET}}$). A distinct threshold voltage for the transition into a conducting state as in conventional diffusive memristors is observed, when at voltages $V > V_{\text{SET}}$ the driving forces causing filament decay are compensated. Filaments are more resilient toward spontaneous decay when they have a larger diameter.^[31] In previous work, this conventional diffusive memristive switching behavior could also be observed at the level of a single Ag-based alloy nanoparticle, which was probed by cAFM.^[32] In contrast, the intermediate-scale AgPt-NP system, which was investigated in this work, does not exhibit distinct threshold voltages. Instead, after the first switching event to a conducting state (i.e., notably at voltages $V > V_{\text{SET}}$) within one measurement cycle, repetitive decays, and reformations of the conducting state are observed, leading to an irregular spiking pattern. The occurrence of multiple, correlated switching events (i.e., ISEs) per cycle, constitutes a further increase in the volatility of the filamentary conduction and as such a shift from conventional diffusive switching toward a highly volatile regime.

We hypothesize, that such dynamics can be observed, when neither the excitatory-like nor inhibitory-like mechanism acting on the filamentary structures is dominant, but rather balanced, causing morphological fluctuations of the filament, which repetitively opens and closes a conducting path. To support this hypothesis, the transition from conventional diffusive memristive behavior toward highly volatile switching (see Supporting Information S5) was reproduced in a lookup-table model based on experimental data from a single SiO₂/AgPt-NP/SiO₂ junction.^[32] As the applied serial resistance effectively limits excitatory contributions when the device is in a conducting state, the transition toward a highly volatile regime is observed when the serial resistance was increased. This corroborates that via precise tailoring of the balance between excitatory and inhibitory contributions different operational regimes of diffusive memristive systems can be obtained.

4.2. Similarities to Neuronal Behavior

Interestingly, the highly volatile memristive regime observed in this work resembles operational principles on the level of a few neurons in biological neuronal systems, which is discussed in the following. In certain neuronal configurations, excitatory and inhibitory synaptic inputs play a crucial role in the activity of an individual neuron. This is emphasized in **Figure 5** (left) by a typical feedback inhibition configuration.^[35,54] A neuron (E1) receives an input, causing it to excite an adjacent neuron

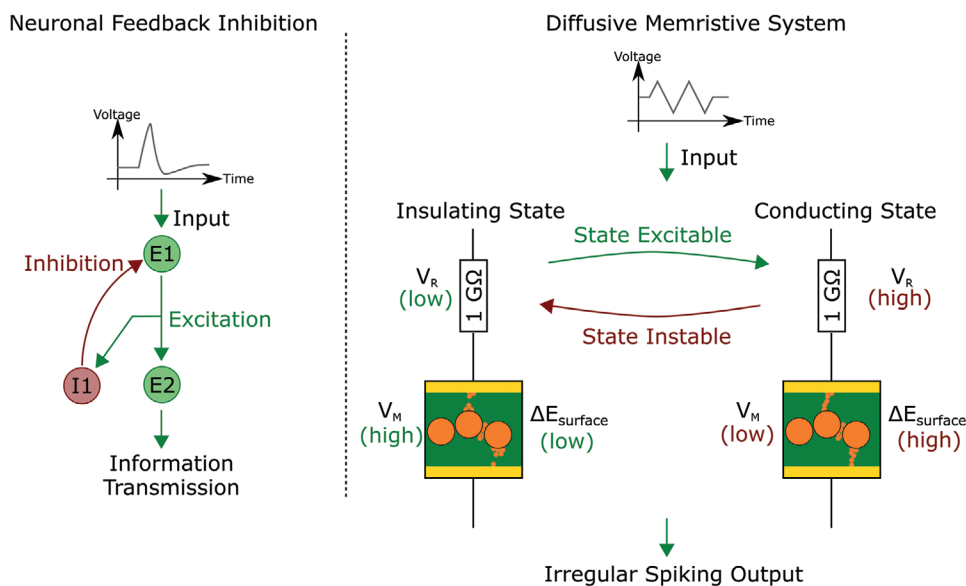


Figure 5. Analogy between neuronal feedback inhibition circuit and diffusive memristive systems in a highly volatile regime. Left: Illustration of feed-back inhibition, which substantially contributes to information representation and processing in biological neuronal systems.^[35,54] An Input (sketched as an action potential) arrives at neuron E1, which in turn excites neurons E2 and I1. E2 is responsible for a feedforward flow of information, whereas I2 incorporates a feedback loop that inhibits the activity of E1 (meaning that activity of E1 causes its own inhibition). Right: Representation of driving forces acting on the memristive system. Starting with the insulating state (i.e., no continuous filament exists), when an external voltage is applied, the majority of the electrical field drops across the memristive system (V_R/V_M denotes the field across the serial resistor/ memristive system), which excites the formation of a filament. In the conducting state, V_M is low and interfacial energy in the system $\Delta E_{\text{surface}}$ gets increased due to filamentary structures, both promoting the instability of the conducting state. Hence, when the memristive system switching into the conducting state, the filamentary structures are inherently destabilized.

(E2), which denotes regular information transmission in biological neuronal system. Besides excitation of E2, a recurrent connection (I1) gets also excited, which again inhibits the excitability of neuron E1. All in all, the fact, that neuron E1 transmits information within a neuronal network, inherently triggers its own inhibition. We argue that such kind of behavior can be imitated by the physical mechanisms acting during the highly volatile operation regime of a filamentary memristive system. Figure 5 (right) depicts the scenario for a memristive system in analogy to the neuronal configuration. When an input (e.g., voltage signal) is received by the memristive system, transmission of information may be triggered (i.e., switching to a conducting state). As a consequence, this shifts the electrical field across the serial resistor and the inhibitory-like mechanisms now significantly contribute to the state of the memristive system. However, we note that the strength of inhibition on the memristive system cannot be readjusted arbitrarily, which is a prominent deviation in the analogy to neuronal systems.^[55,56] A short discussion on this is given in Supporting Information S8.

In biological neuronal systems, the excitatory and inhibitory contributions are inseparable, and especially to have a balance between both, has major importance for the computational capabilities.^[35,46] Biological neuronal systems optimize the ratio of excitatory and inhibitory contributions, to reach an activity level of neurons with a maximized dynamical range.^[18,34] The dynamical range can be understood as the number of different spiking patterns a population of neurons can show evoked by stimulation.^[13] If a neuronal population could only occupy a few different activity patterns (i.e., dynamical range is low), this population would have no chance to represent a broad range

of information, which is strongly obstructive for computation. When excitation within the biological neuronal system would be highly dominating, any evoked activity would trigger highly correlated and exploding activity between neurons, which makes separation of the evoking stimulus difficult (on the other extreme, a too high degree of inhibition would suppress any information transmission). For this reason, in biological neuronal systems, the activity is regulated by inhibitory contributions, to increase the dynamical regime of neurons to bring the whole network into a state which is most efficient for information representation and transmission.

In a similar way, as inhibition increases the dynamical range in biological neuronal systems, the pronounced impact of physical forces causing repetitive decay of conducting states also strongly increases the dynamical range of the memristive system. By this, a broad range of spiking patterns can be realized with a nanoscale memristive system, in close resemblance to the behavior of neurons. This enhances the role of diffusive memristive systems for the design of neuromorphic systems by the strategy, to increase the dynamical range through confinement in a highly volatile switching regime. We note that such behavior cannot be conceived by typical neuron models or be readily applied in artificial neuronal networks. However, it could be interesting, to explore this strategy for applications in reservoir computing, which requires that information input (having a spatio-temporal nature) is mapped into a higher-order complex space, called a reservoir.^[26,57] Recently, it was demonstrated that diffusive memristive systems are suitable as network elements to create a reservoir.^[58] Overall, considering that the dynamic range of diffusive switching can be increased

when the memristive system is operated in a highly volatile regime, similarly as it is done in biology through balancing excitatory and inhibitory contributions, enhanced strategies for engineering reservoirs with improved computational capabilities could be realized.

5. Conclusion and Outlook

In summary, the memristive switching dynamics of an intermediate-scale AgPt NP assembly were investigated via cAFM under constraint operation in a highly volatile regime. Establishment of the high volatility was reached through measures (incorporation of 1 GΩ serial resistor, limited reservoir of Ag, operation under a triangular voltage signal) which strongly limits the Ag-mass transport. The memristive switching was governed by repetitive formation and decay of conducting states, resulting in a highly dynamical regime resembling the irregular spiking patterns of neurons in biological neuronal systems. To describe this regime, we introduced “inhibitory-like” spiking events as probabilistic decays of conducting states at voltages above the threshold voltage for diffusive switching. By this, the investigated dynamics can be understood as an extension of conventional diffusive switching toward an increased dynamical range, which could provide computational benefits for the design of neuromorphic systems. This was argued by the close resemblance to the behavior of individual neurons in biological neuronal systems, where the dynamics are shaped through a balance of excitatory and inhibitory contributions in order to tune the system into a dynamical regime that has a high potential for bio-inspired computation.

This study demonstrates on a fundamental level that intermediate-scale filamentary memristive systems can be constrained into a highly diffusive regime, which may prove interesting for a later transfer to real device implementation. Engineering devices that implement the highly volatile operation regime could be useful for the physical implementation of reservoir computing substrates.^[26] To pave the way for this, more detailed studies on the kinetics acting on the volatile filament (and especially the interplay between different physical forces) are required, such as presented here.^[43] All in all, due to the apparent dynamical similarities to excitatory and inhibitory synaptic contributions (that are increasing and decreasing neuronal firing, respectively), this work provides novel perspectives for the design of neuromorphic systems.

6. Experimental Section

Sample Fabrication: A commercially available Pt-coated cantilever (Bruker CONTV-PT) was loaded to a high-vacuum physical vapor deposition system, that was equipped with two independent sources for SiO_xN_y and AgPt NP deposition. The orientation of the cantilever inside the deposition chamber was adjusted in such a way, that the cantilever apex was oriented toward the SiO_xN_y source and one edge of the pyramid geometry was oriented toward the AgPt NP source. This orientation led to a sample structure as shown in Figure 1. A schematic depiction of the memtip cantilever fabrication setup can be found in Figure S1c, Supporting Information). The SiO_xN_y layers were fabricated

by DC reactive sputtering under a gas mixture of 50 sccm Ar and 0.44 sccm N₂. Slight oxidation of the as-deposited SiN_x upon exposure to ambient atmosphere was expected, which consequently led to the formation of SiO_xN_y. AgPt NPs were deposited by a Haberland-type gas aggregation source (GAS) (details of NP deposition are reported in earlier studies^[59]). The fabrication of the memtip samples was performed via sequential deposition steps. First, a 5 nm SiO_xN_y layer was deposited, followed by a deposition of AgPt NPs were deposited. After confirming the applicability of the sample via SEM (it has to be ensured, that the active region around the apex had a proper coverage of NPs forming the memristive system), in another deposition step a 5 nm SiO_xN_y layer covering the AgPt NPs was deposited in a second vacuum step.

Data Acquisition: The IV characteristics were acquired by a conventional cAFM electrical setup with the exception of adding a serial resistor of 1 GΩ to limit the current within sub-nanoamp range. To minimize the pickup and other unwanted electrical noise the preamplifier was placed close to the sample (≈1 cm away) and in addition, all cables and sample area were shielded to the circuit ground. The preamplifier had a gain of 10⁹ and was capable of measuring currents from 2 pA up to 1 μA at a minimum acquisition time of 20 μs per data point. A typical IV cycle was acquired at a rate of 0.3 Hz. Commercially available Au(111) had been used on mica as a counter electrode that was purchased from Phasis Sàrl, Switzerland. The sample cleanliness was verified by cAFM prior to measurements to ensure its suitability for long-term data acquisition. In case of any visualized defects, the sample was cleaned by two sputtering and annealing cycles. However, all fresh substrates did not require such an extra step. No forming operation was done before measuring the memristive system.

Data Evaluation: A Python script was applied to extract the ISEs (i.e. “inhibitory-like” spiking events) from the raw data. First, the raw data was converted to a conductance versus time representation, as shown in Figure 2b,c. For a more convenient presentation of data, data points belonging to sequences where positive voltages were applied a discarded, because they did not exhibit any memristive activity. Nevertheless, it must be considered that these periods had a meaning for the physical behavior of the system because these were periods where the intermediate-scale AgPt NP system was allowed to relax. Moreover, during the conversion to the conductance versus time representation, all conductance values below 0.01 nS were set to an equal level of 0.01 nS and slight smoothing via a Savitzky-Golay filter with lowest possible window length of 3 was performed. An ISE was detected in the conductance versus time representation, whenever the conductance (starting from a conductive state) exhibited a monotonic decrease over at least one order of magnitude. It was estimated that this definition of an ISE was rather conservative and it could be assumed, that more ISE-causing conductance dropped below one order of magnitude were present in the data. For the ISE count statistics in Figure 3a, a histogram with logarithmic bin widths was calculated. The autocorrelation function ρ_k in Figure 3c was calculated according to^[48]

$$\rho_k = \frac{\frac{1}{N-k-1} \sum_{i=k+1}^N (x_i - \mu)(x_{i-k} - \mu)}{\frac{1}{N-1} \sum_{i=1}^N (x_i - \mu)^2} \quad (1)$$

where k is the lag of measurement cycles, $N = 8000$ is the total number of measurement cycles, x_i is the number of ISEs in a cycle i and μ is the total mean of all ISEs. An IEI (i.e. interevent-interval) was defined as time between two consecutive ISEs. IEIs were only calculated within one measurement cycle, i.e., there are no IEIs between more than one measurement cycle possible. The PDF of IEIs in Figure 4 was estimated by logarithmic binning.

Supporting Information

Supporting Information is available from the Wiley Online Library or from the author.

Acknowledgements

Funded by the Deutsche Forschungsgemeinschaft (DFG, German Research Foundation) – Project-ID 434434223 – SFB 1461. A.H. would like to acknowledge the financial support by the Slovenian Research Agency (ARRS) under Program No. P1-0099 and support for his research stay in Kiel by SFB 1461.

Open access funding enabled and organized by Projekt DEAL.

Conflict of Interest

The authors declare no conflict of interest.

Author Contributions

N.C., T.S., F.F., A.H., and A.V. conceived the studies on cantilevers decorated with intermediate-scale AgPt-NP-based memristive systems. N.C. and A.V. fabricated the functionalized cantilevers in this work. N.C. and A.V. performed the SEM measurements. A.H. performed the cAFM measurements of the functionalized cantilevers. N.C., A.H., and A.V. evaluated the highly volatile switching dynamics and elaborated on the statistical description. A.V. conceived the lookup-table model based on diffusive switching in Supporting Information S5. N.C. wrote the original draft of the manuscript. T.S., F.F., A.H., and A.V. reviewed and edited the manuscript. A.V. supervised the work of N.C. F.F. and A.V. acquired funding for the project.

Data Availability Statement

The data that support the findings of this study are available from the corresponding author upon reasonable request.

Keywords

conductive atomic force microscopy, diffusive memristors, nanoparticles, neuromorphic computing, spiking memristors

Received: July 15, 2022

Revised: November 23, 2022

Published online: January 19, 2023

- [1] M A. Zidan, J. P. Strachan, W D. Lu, *Nat. Electron.* **2018**, 1, 22.
- [2] J. J. Yang, D B. Strukov, D R. Stewart, *Nat. Nanotechnol.* **2013**, 8, 13.
- [3] A H. Edwards, H J. Barnaby, K A. Campbell, M N. Kozicki, W. Liu, M J. Marinella, *Proc. IEEE* **2015**, 103, 1004.
- [4] J. Zhu, T. Zhang, Y. Yang, Ru Huang, *Appl. Phys. Rev.* **2020**, 7, 011312.
- [5] Z. Wang, L. Wang, M. Nagai, L. Xie, M. Yi, W. Huang, *Adv. Electron. Mater.* **2017**, 3, 1600510.
- [6] V K. Sangwan, M C. Hersam, *Nat. Nanotechnol.* **2020**, 15, 517.
- [7] Q. Xia, J. J. Yang, *Nat. Mater.* **2019**, 18, 309.
- [8] D. Ielmini, H.-S. P. Wong, *Nat. Electron.* **2018**, 1, 333.
- [9] P. Yao, H. Wu, B. Gao, S. B. Eryilmaz, X. Huang, W. Zhang, Q. Zhang, N. Deng, L. Shi, H.-S. P. Wong, He Qian, *Nat. Commun.* **2017**, 8, 15199.
- [10] A. Serb, J. Bill, A. Khait, R. Berdan, R. Legenstein, T. Prodromakis, *Nat. Commun.* **2016**, 7, 12611.
- [11] M. Prezioso, F. Merrih-Bayat, B. D. Hoskins, G. C. Adam, K. K. Likharev, D. B. Strukov, *Nature* **2015**, 521, 61.
- [12] D R. Chialvo, *Nat. Phys.* **2010**, 6, 744.
- [13] W L. Shew, D. Plenz, *Neuroscientist* **2013**, 19, 88.
- [14] R C. Froemke, *Annu. Rev. Neurosci.* **2015**, 38, 195.
- [15] S. Zhou, Y. Yu, *Front Neurosci* **2018**, 12, 1.
- [16] S. Denā`Ve, C. K. Machens, *Nat. Neurosci.* **2016**, 19, 375.
- [17] Y. Dan, Mu-M Poo, *Neuron* **2004**, 44, 23.
- [18] W. L. Shew, H. Yang, S. Yu, R. Roy, D. Plenz, *J. Neurosci.* **2011**, 31, 55.
- [19] L. Yu, Z. Shen, C. Wang, Y. Yu, *Front Cell Neurosci* **2018**, 12, 1.
- [20] K. Linkenkaer-Hansen, V V. Nikouline, J. M. Palva, R. J. Ilmoniemi, *J. Neurosci.* **2001**, 21, 1370.
- [21] J M. Beggs, D. Plenz, *J. Neurosci.* **2003**, 23, 11167.
- [22] J. Hochstetter, R. Zhu, A. Loeffler, A. Diaz-Alvarez, T. Nakayama, Z. Kuncic, *Nat. Commun.* **2021**, 12, 4008.
- [23] M D. Pike, S K. Bose, J B. Mallinson, S K. Acharya, S. Shirai, E. Galli, S J. Weddell, P J. Bones, M D. Arnold, S A. Brown, *Nano Lett.* **2020**, 20, 3935.
- [24] J. B. Mallinson, S. Shirai, S. K. Acharya, S. K. Bose, E. Galli, S. A. Brown, *Sci. Adv.* **2019**, 5, aaw8438.
- [25] S. Shirai, S. K. Acharya, S. K. Bose, J. B. Mallinson, E. Galli, M D. Pike, M D. Arnold, S. A. Brown, *Netw Neurosci* **2019**, 4, 432.
- [26] G. Tanaka, T. Yamane, J. B. HÄ©roux, R. Nakane, N. Kanazawa, S. Takeda, H. Numata, D. Nakano, A. Hirose, *Neural Networks* **2019**, 115, 100.
- [27] G. Milano, G. Pedretti, K. Montano, S. Ricci, S. Hashemkhani, L. Boarino, D. Ielmini, C. Ricciardi, *Nat. Mater.* **2021**, 21, 195.
- [28] Z. Wang, M. Rao, R. Midya, S. Joshi, H. Jiang, P. Lin, W. Song, S. Asapu, Ye Zhuo, C. Li, H. Wu, Q. Xia, J. J. Yang, *Adv. Funct. Mater.* **2018**, 28, 1704862.
- [29] R. Wang, J.-Q. Yang, J.-Yu Mao, Z.-P. Wang, S. Wu, M. Zhou, T. Chen, Ye Zhou, Su-T Han, *Adv Intell Syst* **2020**, 2, 2000055.
- [30] Z. Wang, S. Joshi, S E. Savelä Ev, H. Jiang, R. Midya, P. Lin, M. Hu, N. Ge, J. P. Strachan, Z. Li, Q. Wu, M. Barnell, G.-L. Li, H L. Xin, R. S. Williams, Q. Xia, J. J. Yang, *Nat. Mater.* **2017**, 16, 101.
- [31] W. Wang, M. Wang, E. Ambrosi, A. Bricalli, M. Laudato, Z. Sun, X. Chen, D. Ielmini, *Nat. Commun.* **2019**, 10, 81.
- [32] A. Vahl, N. Carstens, T. Strunskus, F. Faupel, A. Hassanien, *Sci. Rep.* **2019**, 9, 17367.
- [33] R. Midya, Z. Wang, S. Asapu, S. Joshi, Y. Li, Ye Zhuo, W. Song, H. Jiang, N. Upadhyay, M. Rao, P. Lin, C. Li, Q. Xia, J. J. Yang, *Adv. Electron. Mater.* **2019**, 5, 1900060.
- [34] G. Deco, A. Ponce-Alvarez, P. Hagmann, G. L. Romani, D. Mantini, M. Corbetta, *J. Neurosci.* **2014**, 34, 7886.
- [35] J. S. Isaacson, M. Scanziani, *Neuron* **2011**, 72, 231.
- [36] W. L. Shew, H. Yang, T. Petermann, R. Roy, D. Plenz, *J. Neurosci.* **2009**, 29, 15595.
- [37] N. Carstens, A. Vahl, O. Gronenberg, T. Strunskus, L. Kienle, F. Faupel, A. Hassanien, *Nanomaterials* **2021**, 11, 265.
- [38] W. Li, X. Song, X. Zhao, X. Zhang, R. Chen, X. Zhang, C. Jiang, J. He, X. Xiao, *Nano Energy* **2020**, 67, 104213.
- [39] H. J. Kim, T. H. Park, K. J. Yoon, W Mo Seong, J. W. Jeon, Y. J. Kwon, Y. Kim, D. E. Kwon, G. S. Kim, T. J. Ha, S. G. Kim, J. Ho Yoon, C. S. Hwang, *Adv. Func. Mater.* **2019**, 29, 1806278.
- [40] B. K. You, J. M. Kim, D J. Joe, K. Yang, Y. Shin, Y. S. Jung, K. J. Lee, *ACS Nano* **2016**, 10, 9478.
- [41] M. Lanza, H.-S. P. Wong, E. Pop, D. Ielmini, D. Strukov, B C. Regan, L. Larcher, M A. Villena, J. J. Yang, L. Goux, A. Belmonte, Y. Yang, F M. Puglisi, J. Kang, B. Magyar-Köpe, E. Yalon, A. Kenyon, M. Buckwell, A. Mehonic, A. Shluger, H. Li, T.-H. Hou, B. Hudec, D. Akinwande, R. Ge, S. Ambrogio, J B. Roldan, E. Miranda, J. Suñe, K. L. Pey, et al., *Adv. Electron. Mater.* **2019**, 5, 1800143.
- [42] Y. Yang, Ru Huang, *Nat. Electron.* **2018**, 1, 274.
- [43] S. A. Chekol, S. Menzel, R. W. Ahmad, R. Waser, S. Hoffmannä Eifert, *Adv. Funct. Mater.* **2021**, 32, 2111242.
- [44] S. Menzel, S. Tappertzhofen, R. Waser, I. Valov, *Phys. Chem. Chem. Phys.* **2013**, 15, 6945.
- [45] M N. Shadlen, W T. Newsome, *Curr. Opin. Neurobiol.* **1994**, 4, 569.

- [46] M. N. Shadlen, W. T. Newsome, *J. Neurosci.* **1998**, *18*, 3870.
- [47] C. F. Stevens, A. M. Zador, *Nat. Neurosci.* **1998**, *1*, 210.
- [48] A. Eke, P. Herman, L. Kocsis, L. R. Kozak, *Physiol Meas* **2002**, *23*, R1.
- [49] G. Buzsáki, K. Mizuseki, *Nat. Rev. Neurosci.* **2014**, *15*, 264.
- [50] V. G. Karpov, D. Niraula, *IEEE Electron Device Lett.* **2017**, *38*, 1240.
- [51] S. K. Acharya, E. Galli, J. B. Mallinson, S. K. Bose, F. Wagner, Z. E. Heywood, P. J. Bones, M. D. Arnold, S. A. Brown, *ACS Appl. Mater. Interfaces* **2021**, *13*, 52861.
- [52] B. Cho, J.-M. Yun, S. Song, Y. Ji, D.-Yu Kim, T. Lee, *Adv. Funct. Mater.* **2011**, *21*, 3976.
- [53] R. Waser, R. Dittmann, G. Staikov, K. Szot, *Adv. Mater.* **2009**, *21*, 2632.
- [54] D. M. Kullmann, *Curr. Opin. Neurobiol.* **2011**, *21*, 709.
- [55] G. Mongillo, S. Rumpel, Y. Loewenstein, *Nat. Neurosci.* **2018**, *21*, 1463.
- [56] N. Sukenik, O. Vinogradov, E. Weinreb, M. Segal, A. Levina, E. Moses, *Proc. Natl. Acad. Sci. USA* **2021**, *118*, 2018459118.
- [57] M. Lukoševičius, H. Jaeger, *Comput. Sci. Rev.* **2009**, *3*, 127.
- [58] R. Midya, Z. Wang, S. Asapu, X. Zhang, M. Rao, W. Song, Ye Zhuo, N. Upadhyay, Q. Xia, J. J. Yang, *Adv. Intell. Syst.* **2019**, *1*, 1900084.
- [59] A. Vahl, J. Strobel, W. Reichstein, O. Polonskyi, T. Strunskus, L. Kienle, F. Faupel, *Nanotechnology* **2017**, *28*, 175703.